Dual hit rat models of diabetic cardiomyopathy and nephropathy: pancreatectomy combined with isoprenaline treatment or uninephrectomy

Louise Thisted (lth@gubra.dk)
Gubra Aps https://orcid.org/0000-0002-7783-8122
Mette V Østergaard
Gubra Aps
Annemarie A Pedersen
Gubra Aps
Philip J Pedersen
Gubra Aps
Ross T Lindsay
University of Cambridge
Andrew J Murray
University of Cambridge
Lisbeth N Fink
Gubra Aps
Tanja X Pedersen
Gubra Aps
Thomas Secher
Gubra Aps
Thea T Johansen
Gubra Aps
Sebastian T Thrane
Gubra Aps
Torben Skarsfeldt
Serodus ASA
Jacob Jelsing
Gubra Aps
Morten B Thomsen
Kobenhavns Universitet Sundhedsvidenskabelige Fakultet
Nora E Zois
Gubra Aps

Original investigation

Keywords: Preclinical model, hyperglycemia, heart, kidney, microvascular disease, echocardiography, glomerular filtration rate, RNA sequencing, rodent.

Posted Date: April 3rd, 2020

DOI: https://doi.org/10.21203/rs.3.rs-19735/v1

Dual hit rat models of diabetic cardiomyopathy and nephropathy: pancreatectomy combined with isoprenaline treatment or uninephrectomy

Louise Thisted[1,2], Mette V. Østergaard[1], Annemarie A. Pedersen[1], Philip J. Pedersen[1], Ross T. Lindsay[1,3,*], Andrew J. Murray[3], Lisbeth N. Fink[1], Tanja X. Pedersen[1,**], Thomas Secher[1], Thea T. Johansen[1,***], Sebastian T. Thrane[1], Torben Skarsfeldt[4], Jacob Jelsing[1], Morten B. Thomsen[2], Nora E Zois[1].

[1]Gubra Aps, Hørsholm, Denmark

[2]Dept. of Biomedical Sciences, University of Copenhagen, Copenhagen, Denmark

[3]Dept. of Physiology, Development and Neuroscience, University of Cambridge, Cambridge, UK.

[4]Serodus ASA, Oslo, Norway

*Current affiliation: CVRM, AstraZeneca, Gaithersburg, Maryland, USA

**Current affiliation: CVD Research, Novo Nordisk, Måløv, Denmark

***Current affiliation: Dept. of Biomedicine, Aarhus University, Aarhus, Denmark

Corresponding author: Nora Elisabeth Zois, Gubra Aps, In vivo pharmacology, Hørsholm Kongevej 11b, 2970 Hørsholm, Denmark, +45 6170 9037, nez@gubra.dk

ABSTRACT

Background

Cardiovascular and renal complications are the predominant causes of morbidity and mortality amongst patients with diabetes. Development of novel treatments have been hampered by the lack of available animal models recapitulating the human disease. We hypothesized that experimental diabetes in rats combined with a cardiac or renal stressor, would mimic diabetic cardiomyopathy and nephropathy, respectively.

Methods

Diabetes was surgically induced in male Sprague Dawley rats by 90% pancreatectomy (Px). Isoprenaline (Iso, 1 mg/kg, sc., 10 days) was administered five weeks after Px with the aim of inducing cardiomyopathy, and cardiac function and remodeling was assessed by echocardiography ten weeks after surgery. Left ventricular (LV) fibrosis was quantified by Picro Sirius Red and gene expression analysis. Nephropathy was induced by Px combined with uninephrectomy (Px-UNx). Kidney function was assessed by measurement of glomerular filtration rate (GFR) and urine albumin excretion, and kidney injury was evaluated by histopathology and gene expression analysis.

Results

Px resulted in stable hyperglycemia, hypoinsulinemia, decreased C-peptide, and increased glycated hemoglobin (HbA1c) compared with sham-operated controls. Moreover, Px increased LV mass and dimensions, and caused a shift from α-myosin heavy chain (MHC) to β-MHC gene expression. Isoprenaline treatment, but not Px, decreased ejection fraction and induced LV fibrosis. There was no apparent interaction between Px and Iso treatment. The superimposition of Px and UNx increased GFR, indicating hyperfiltration. Compared with sham-operated controls, Px-UNx induced albuminuria and increased urine markers of kidney injury, including neutrophil gelatinase-associated lipocalin (NGAL) and podocalyxin, concomitant with upregulated renal gene expression of NGAL and kidney injury molecule 1 (KIM-1).

Conclusion

Whereas Px and isoprenaline separately produced clinical endpoints related to diabetic cardiomyopathy, the combination of the two did not accentuate disease development. Conversely, Px in combination with UNx resulted in several clinical hallmarks of diabetic nephropathy indicative of early disease development.

KEY WORDS (3-10 words)

Preclinical model, hyperglycemia, heart, kidney, microvascular disease, echocardiography, glomerular filtration rate, RNA sequencing, rodent.

BACKGROUND

Diabetes is a global disorder presently affecting 463 million people worldwide and the prevalence is increasing at alarming rates [1]. Moreover, diabetes is strongly associated with both cardiovascular and renal complications, which are significantly implicated in premature death among these patients [2,3]. Long-term diabetes increases the risk of cardiovascular disease, including myocardial infarction, stroke, and hypertension [4–6]. Independently, patients with diabetes also experience structural and functional abnormalities of the myocardium defined as diabetic cardiomyopathy (DbCM) [7,8]. The clinical manifestation of DbCM includes myocardial dilatation and hypertrophy, left ventricular (LV) dysfunction, and interstitial fibrosis [8–10]. The underlying mechanism is still incompletely understood but aside from metabolic derangements, microvascular dysfunction has been implicated [7,11]. Microvascular changes are also implicated in diabetic nephropathy (DN), which occurs in up to 40% of patients with diabetes. In addition to being associated with increased cardiovascular mortality, DN is also the leading cause of chronic and end-stage kidney disease [12]. The main clinical manifestations of DN are persistent albuminuria and decreased glomerular filtration rate (GFR) [13], while additional hallmarks include renal hypertrophy, loss of podocytes, glomerulosclerosis, and tubulointerstitial fibrosis [14,15]. Nonetheless, DN is a heterogeneous kidney disease exhibiting variability in the degree of albuminuria, histopathological features, and different disease trajectories.

Further insight into the pathogenesis of both DbCM and DN is essential in order to advance clinical management of these major causes of morbidity and mortality worldwide. According to the Diabetic Complications Consortium, a valid rodent model of DbCM should include left ventricular (LV) dysfunction and hypertrophy, interstitial fibrosis, and altered gene expression, but also an increased vulnerability to cardiac stressors [16]. For DN, a valid model should comprise progressive albuminuria and GFR loss, alongside characteristic histopathological changes such as arteriolar hyalinosis, glomerulosclerosis, and tubulointerstitial fibrosis [17]. The most-studied, current rodent models of diabetic complications are often limited in their

usefulness as they produce only a few essential features associated with early stages of DbCM and DN progression [18–20]. Some of these commonly-used models of diabetes, e.g. streptozotocin-treatment (STZ) and the *db/db* genetic mouse model, have previously been combined with angiotensin II or uninephrectomy to mimic and accelerate DbCM or DN, respectively [21–23].

The use of STZ in this context is however suboptimal, since the toxin also has the potential to induce direct nephrotoxic and cardiotoxic effects, independent of hyperglycemia [24–26]. Pancreatectomy (Px), on the other hand, is a well-characterized method of surgically inducing diabetes in rats [27]. An important advantage of this model is that it reflects the isolated effects of a reduced beta cell mass; immediately after surgery Px rats become insulin deficient and hyperglycemic, allowing full control of diabetic onset [28]. To our knowledge, the cardiac and renal pathology has not previously been evaluated in the Px rat, and nor have models of DbCM and DN been superimposed upon this model. The aim of this study was therefore to investigate the development and progression of DbCM and DN in a Px rat model of diabetes. To accentuate the cardiac and renal changes, we combined Px with isoprenaline, a non-selective β-adrenoreceptor agonist and well-known cardiac stressor capable of inducing cardiac dysfunction and fibrosis [29–31], and uninephrectomy, which is known to accelerate the progression of injury in the remaining kidney [32,33]. We hypothesized that superimposing these cardiac or renal stressors on pre-existing diabetes would result in rat models that recapitulated key features of human DbCM and DN, respectively.

MATERIALS AND METHODS

Animals

Male Sprague-Dawley rats (NTac:SD) (8-10 weeks old, 210-280 g, Taconic Biosciences) were single-housed in a controlled environment (20-22°C, humidity 40-60%) with a 12h light/dark cycle. The animals were acclimatized for at least one week before surgery. All animals had *ad libitum* access to regular chow diet (Altromin 1324, Brogaarden) and tap water throughout the study period. The studies were approved by The Danish Animal Experiments Inspectorate (license no. 2019-15-0201-01648, 2017-15-0201-01183, 2017-15-0201-01286) and conformed to the European Parliament Directive on the Protection of Animals Used for Scientific Purposes (2010/63/EU).

Experimental design

Three separate experiments were conducted in three cohorts of rats (fig. 1). Experiment 1 involved metabolic characterization of the Px rat model and included sham surgery (n=10), 60% Px (n=10), and 90% Px (n=10). Experiment 2 evaluated the 90% Px and isoprenaline-treated rat as a model of DbCM, and included sham-vehicle (Sham-Veh, n=10), Px-vehicle (Px-Veh, n=15), sham-isoprenaline (Sham-Iso, n=12), Px-isoprenaline (Px-Iso, n=18) groups. Experiment 3 investigated the renal phenotype of the 90% Px and uninephrectomized rat model of DN in sham-operated (n=11) and Px and uninephrectomized rats (Px-UNx, n=12). In experiments 2 and 3, only Px rats exhibiting fasted or fed blood glucose above 10 or 12 mmol/L, respectively, two weeks post-Px were included.

Pancreatectomy

Rats were fasted overnight and received subcutaneous injections of atropine (0.1 mg/kg), enrofloxacin (50 mg/kg), carprofen (50 mg/kg) and saline (20 ml/kg) prior to surgery. All surgical interventions were performed under isoflurane anesthesia (2-3%).

Pancreatectomy. Through a midline abdominal incision, the pancreatic tissue was removed by gentle abrasion with disposable micro-brushes (Plandent). All major blood vessels were left intact. For 60% Px, the tail and body of the pancreas was removed whereas the pancreatic tissue within the duodenal loop, comprising the entire head of the pancreatic tissue, was preserved. For 90% Px, only the pancreatic tissue between the common bile duct extending to the first loop of the duodenum was preserved.

Sham surgery. Through a midline abdominal incision, the tail and body of the pancreatic tissue was disengaged from the mesentery and gently manipulated before being repositioned to the abdominal cavity.

The rats were fasted until the next day, whereupon 5 g of chow was administered to each animal. Two days after surgery, the animals were fed *ad libitum*.

Isoprenaline treatment

Isoprenaline hydrochloride (Sigma-Aldrich) was dissolved in saline immediately prior to dosing and administered subcutaneously (1 mg/kg) for ten consecutive days beginning five weeks after sham surgery or 90% Px.

Uninephrectomy

Animals were subjected to uninephrectomy at the time of 90% Px. The right ureter, renal artery and vein were identified and ligated. Subsequently, the right kidney was removed. In sham-operated animals, the right kidney was exposed and gently manipulated.

Blood and plasma analyses

Blood glucose. Tail vein blood was collected once weekly from non-fasted or fasted (4 h) rats into heparinized glass capillary tubes and immediately suspended in glucose/lactate system solution buffer (EKF-diagnostics). The glucose concentration was measured immediately using a BIOSEN c-Line glucometer (EKF-diagnostics) according to the manufacturer's instructions.

Oral glucose tolerance test (OGTT). In experiment 1, animals were fasted for 4 h prior to oral glucose administration (2 g/kg body weight, 500 mg glucose/mL, Fresenius Kabi), and blood glucose was measured at 6 timepoints over the course of 240 min post-injection.

Blood and plasma markers. Plasma insulin and C-peptide were measured in duplicate using AlphaLISA platform (Perkin Elmer) according to the manufacturer's instructions. Glycated haemoglobin (HbA1c), plasma creatinine, and urea were measured using commercial assays (Roche Diagnostics) on the Cobas C-501 autoanalyzer, and plasma cystatin C was measured using a commercial assay (R&D Systems) all as per manufacturers' instructions.

Urine collection and biochemical analyses

Rats were single-housed in metabolic cages (Techniplast) with free access to powdered chow and water. The excreted urine was collected for 16 hours. Urine creatinine was quantified using a CREP2 assay (Roche Diagnostics) on the Cobas C-501 autoanalyzer as per manufacturer's instructions. Urine albumin was measured using a rat albumin ELISA (Bethyl Laboratories). Urine neutrophil gelatinase-associated lipocalin (NGAL), soluble tumor necrosis factor receptors (sTNFR) I and II were measured using ELISA assays (R&D Systems), while urine nephrin and podocalyxin were quantified using ELISA assays from LSBio and CusaBio, respectively. All ELISA assays were run as per manufacturers' instructions and levels of analytes were reported as the analyte-to-creatinine ratio (ACR) in urine. Urine ACR values were log10-transformed before statistical analyses.

Echocardiography

Echocardiographic assessments were performed under isoflurane anesthesia (2-3%). After chest hair removal, the rats were positioned in supine position on a heated pad.

Electrocardiogram electrodes (lead II configuration, 3M™) were placed and the rectal temperature was measured before and after examination. All examinations were performed using an ultrasound device (Philips, iE33) with a 12 MHz sector array probe. Function and dimensions of the LV were assessed from parasternal short and apical long axis views. The LV internal diameter (LVID), anterior and posterior wall thickness (LVAW, LVPW) were assessed in systole (LVIDs, LVAWs and LVPWs, respectively) and diastole (LVIDd, LVAWd and LVPWd, respectively) using 2D-guided M-mode in a short axis view at the level of the papillary muscles, according to the leading edge to leading edge principle [34]. The ejection fraction (EF) was calculated using the Teichholz formula [35]. To correct for the difference in LV size, all short axis measurements were normalized to body weight. LV filling (E and A velocity and deceleration time) was measured in the apical 4-chamber long axis view with the sample volume placed at the tip of the mitral valve leaflets using pulsed wave Doppler. Echocardiographic analyses were performed offline using Q-station software (version 3.8.5, Philips). Image acquisitions and analyses were performed by one operator blinded towards identity of the animal.

Glomerular filtration rate measurement

GFR was assessed by a fluorescein isothiocyanate (FITC)-inulin test. Briefly, a 5% solution of FITC-inulin (TdB Consultancy) was prepared in 0.85% saline by heating and overnight dialysis using a Spectra/Por 6 dialysis tube (1 kDa molecular cut-off; Spectrum Labs). The FITC-inulin solution was sterile filtered (0.2 µm syringe filter) before tail vein injections in conscious rats (100 mg/kg). Sublingual blood was collected in heparinized tubes at 8 timepoints over the course of 75 min post-injection. Plasma FITC-inulin concentrations were measured using a plate-reader (CLARIOstar, BMG LABTECH) and GFR was calculated using a two-compartment model from the rate of decay in plasma FITC-inulin as described previously [36] and normalized to body weight.

Histology and stereology

Pancreas. At termination, pancreatic samples from sham, 60% and 90% Px rats were removed *en-bloc* and incubated in 10% neutral buffered formalin until further processing. Pancreatic tissue was carefully dissected, weighed, and processed as previously described [37]. Briefly, pancreas was rolled tightly into strips of gauze before infiltration with paraffin in an automated tissue processor (VIP5, Sakura). The pancreas was then cut into 7-9 systematic uniform random tissue slabs with a razor blade fractionator and embedded in paraffin blocks with the cut surface

down. Subsequently, 5 µm thick sections were cut from each block on a microtome and collected on microscope slides. Immunohistochemistry against beta cells and non-beta cells were performed as a double staining using standard procedures. Briefly, after deparaffinization and microwave oven pretreatment in Tris-EGTA buffer (pH 9), sections were stained for non-beta cells using an antibody cocktail consisting of rabbit anti-glucagon (Phoenix, H-028-02, 1:5000), rabbit anti-somatostatin (Dako, 0566, 1:7500), and rabbit anti-pancreatic polypeptide (Europroxima, B32-1, 1:5000). The antibody cocktail was detected using Envision+ anti-rabbit HRP-coupled polymer system (Dako, K4002) and developed with DAB-Nickel as chromogen. Next, beta cells were stained using a guinea pig anti-insulin antibody (Dako, A0564, 1:6000) followed by a biotinylated secondary donkey anti-guinea pig antibody (Jackson ImmunoResearch 706-065-148, 1:2000). Amplification and development of the insulin staining was performed using the Vectastain ABC elite kit (Vector Laboratories PK6100) and Impact NovaRed (Vector Laboratories, SK-4805). Finally, sections were counterstained with Mayer's hematoxylin (Sigma-Aldrich).

Heart and kidney. One half of the sagittally-divided LV or left kidney were fixed in 10% neutral buffered formalin for 24 h at room temperature. The fixed tissues were cut into 5-7 systematic uniform random tissue slabs with a razor blade fractionator and embedded in paraffin blocks with the cut surface down. For Picro Sirius Red staining, a set of 3 µm sections were cut on a microtome from each block and collected on microscope slides. For Periodic acid-Schiff (PAS) staining, another set of sections were cut in pairs with a dissector distance of 30 µm. Picro Sirius Red staining: After deparaffinization, sections were incubated in Wiegert's iron hematoxylin (Sigma-Aldrich) and then stained in Picro Sirius Red (Sigma-Aldrich) before they were cover slipped with Pertex. For the PAS staining, sections were deparaffinized and oxidized with 0.5% periodic acid solution followed by incubation with Schiff's reagent. Sections were counterstained in Mayer's hematoxylin and cover slipped with Pertex. Podocin/type IV collagen double fluorescent immunohistochemical staining of kidney sections was performed as previously described [22].

Image analysis and stereological quantification. Stereological quantification of beta cell and non-beta cell mass was calculated as an area fraction (area of beta cells versus total pancreatic area) multiplied by the dissected pancreas mass as previously described in [38]. Heart and kidney collagen content was determined as Picro Sirius Red area fraction using image analysis. Stained slides were scanned under a 20x objective in an Aperio Scanscope AT slide scanner and imported into an image analysis module in Visiopharm Integrator System (Visiopharm). A Bayesian classifier was trained to detect Picro Sirius Red positive collagen versus other

tissue components. The collagen area fraction was calculated as the Picro Sirius Red area divided by the total tissue area. Intra-glomerular collagen type 4 content and stereological estimation of kidney compartmental volumes were determined as previously described [22]. The mean glomerular volume was calculated as total glomerular volume divided by the mean number of glomeruli estimated using the physical dissector on serially cut reference and look-up sections with a dissector distance of 30 µm [39].

RNA sequencing

Transcriptome analysis was performed by sequencing of RNA extracts from the LV and renal cortex. RNA was purified from homogenized tissue using the NucleoSpin RNA Plus kit (Macherey-Nagel GmbH). The RNA quantity was measured using Qubit (Thermo Scientific, Eugene, OR) and RNA quality was determined using a bioanalyzer with RNA 6000 Nano kit (Agilent). Purified RNA from each sample was used to generate a cDNA library using the NEBNext Ultra II Directional RNA Library Prep Kit for Illumina (New England Biolabs, Ipswich, MA). cDNA libraries were sequenced on a NextSeq 500 using NextSeq 500/550 High Output Kit V2 (Illumina). Reads were aligned to the Ensembl Rnor_6.0 release 89 *Rattus norvegicus* genome using STAR v.2.5.2a with default parameters [40]. Differential gene expression analysis was performed with DEseq2 [41].

Statistical analysis

All data were analyzed using GraphPad Prism software (version 8.02). Normal distribution of data was assessed by inspection of QQ plots and by using the Shapiro-Wilk test. Normally distributed data are shown as mean ± standard error of mean (SEM). In experiment 1, repeated measures two-way analyses of variance (ANOVA) with Bonferroni's post-hoc test were used for time-course data and one-way ANOVA with Tukey's post-hoc test was used for insulin and beta cell mass data. In experiment 2, two-way ANOVA was applied and in addition to evaluating the main effects of Px and isoprenaline treatment, the interaction between the two was included to evaluate a potential synergistic effect. Unpaired t-test and repeated measurements two-way ANOVA with Bonferroni's Multiple Comparisons test were used for experiment 3. A p-value <0.05 was considered statistically significant.

RESULTS

Metabolic characterization of the pancreatectomized rat

In experiment 1, 60% Px did not affect body weight, whereas 90% Px resulted in a lower rate of body weight gain over 6 weeks compared with sham-operation ($p<0.05$, fig. 2A). One week after surgery, 90% Px rats exhibited hyperglycemia (non-fasting blood glucose > 10 mmol/L) whereas 60% Px and sham rats were normoglycemic ($p<0.05$, fig. 2B). Among the 90% Px rats, 50% remained hyperglycemic throughout the six-week study period (defined as '90% Px responders') whereas 50% returned to normoglycemia three weeks after surgery (defined as '90% Px non-responders'). Correspondingly, blood glucose was increased for 15-120 min after an oral glucose bolus during the OGTT in 90% Px responders compared to sham ($p<0.05$, fig. 2C), but only for 15-30 minutes in 90% Px non-responders and in 60% Px. Both 60% and 90% Px resulted in significantly lower plasma insulin compared with sham ($p<0.05$, fig. 2D). While the total beta cell mass in the remaining pancreatic tissue was reduced in 60% and 90% Px rats compared to sham-operated controls six weeks after surgery ($p<0.01$ and $p<0.001$, respectively, fig. 2E), morphology of the individual islets looked similar across groups (fig. 2F).

The pancreatectomized and isoprenaline-treated rat as a model of DbCM

In experiment 2, one rat was excluded due to lack of hyperglycemia two weeks after Px, five rats died from post-operative complications, and five Sham-Iso rats died after the first administration of isoprenaline (isoprenaline-induced mortality rate: 29.4%).

No significant interaction between Px and isoprenaline treatment was found for any investigated outcome. Instead, irrespective of isoprenaline treatment, a main effect of Px was found for several measures reflecting glucose metabolism and LV remodeling. Specifically, plasma C-peptide and HbA1c were increased post-Px, plasma insulin was decreased, and animals subjected to Px did not gain body weight to the same extent over the following ten weeks as sham-operated animals (Table 1; all $p<0.001$). Heart rate and peak E wave velocity were decreased (Table 2; $p<0.001$) and relative LV mass ($p<0.05$), wall thickness and internal dimensions in systole and diastole (Fig. 3, Table 2; $p<0.001$) was increased in Px rats compared with sham-operated counterparts. Furthermore, LV collagen area fraction was modestly decreased by Px (Table 1; $p<0.05$). Owing to the frequent finding of fused E- and A-waves, calculation of E/A ratios was not possible during echocardiography.

In a manner distinct from Px, isoprenaline treatment decreased indices of systolic LV function; LVIDs and EF (Fig. 3, Table 2; both $p<0.001$) and increased LV collagen area fraction (Table 1, $p<0.001$).

Transcriptome analysis of LV tissue revealed a Px-driven change in expression of genes related to cardiac metabolism and function compared to sham. Specifically, glucose transporter (GLUT) 1, GLUT4, α-myosin heavy chain (MHC), and sarco/endoplasmic reticulum Ca^{2+}-ATPase (SERCA) -2 were all downregulated, whilst β-MHC and uncoupling protein (UCP) 3 were upregulated ($p<0.001$, fig. 4). In contrast, isoprenaline treatment *per se* did not affect gene expression of these selected genes compared to vehicle treatment other than upregulating GLUT1 ($p<0.01$). Further analysis of expression levels of genes involved in adrenergic signaling revealed that β_2-receptors were downregulated by Px ($p<0.01$) while β_1-receptors were unaffected (data not shown). Moreover, expression of downstream mediators of β-receptor signaling, adenylate cyclase (AC) 6 and phosphodiesterase 3A (PDE3A) were upregulated by Px ($p<0.001$ and $p<0.05$, respectively) while PDE3A was downregulated by isoprenaline ($p<0.05$).

The pancreatectomized and uninephrectomized rat as a model of DN

In experiment 2, renal changes induced by Px were observed including increased left kidney weight (1.7±0.1 g vs.1.4±0.1 g, $p<0.05$) and urine ACR (2549±1447 µg/mg vs. 64 ±10 µg/mg, $p<0.01$) in Px-Veh compared to Sham-Veh ten weeks after surgery. This indicates renal pathology in the Px rats. In experiment 3, the progression of DN in Px rats was therefore investigated alongside UNx, a known accelerator of disease progression in rodent models of DN. As expected, Px-UNx caused an increase in blood glucose and a decrease in plasma insulin compared to sham (both $p<0.05$, table 4). Urinary excretion of albumin, NGAL, and sTNFR-II was increased in Px-UNx two weeks after surgery and sustained at six and nine weeks post-surgery (all $p<0.001$, table 3). Urine sTNFR-I and podocalyxin excretion was increased by week six and nine after surgery (both $p<0.001$). At termination, eleven weeks after surgery, plasma urea was increased in Px-UNx ($p<0.05$), whereas plasma creatinine was reduced ($p<0.05$). Cystatin C was not significantly different, but GFR was increased eight weeks after surgery in Px-UNx compared to sham ($p<0.05$).

Renal hypertrophy was observed in Px-UNx rats compared with sham-operated animals with increased kidney weight and renal cortex and medulla volumes ($p<0.05$, fig. 5A-C). Px-UNx rats also displayed significant glomerular hypertrophy as assessed by stereology ($p<0.05$ vs. sham, fig. 5D), in an unaltered number of glomeruli (39,472±1,336 vs 39,130±1,665 glomeruli, ns.). Fibrosis quantification by histopathology showed unchanged levels of renal collagen (fig. 5F), and the area fraction of type IV collagen in the glomeruli was unaffected in Px-UNx rats compared with sham (fig. 5H).

Renal cortex gene expression analysis of selected pathways involved in the pathogenesis of diabetic nephropathy is shown in Figure 6A. Several genes involved in TGF-beta signaling, fibrosis and inflammation, and angiogenesis were upregulated, while the expression of genes involved in the renin-angiotensin-aldosterone system was downregulated (fig. 6A). Genes of the insulin signaling pathway were significantly altered in Px-UNx compared to sham (fig. 6A). Expression of podocyte markers was either down-regulated (nephrin) or unchanged (podocin), while tubular damage markers (neutrophil gelatinase-associated lipocalin (NGAL) and Kidney Injury Molecule-1 (KIM-1)) were significantly upregulated ($p<0.05$, fig. 6B). Finally, drug-related targets including sodium-glucose transport protein 2, glucagon-like peptide 1 receptor, and angiotensin I converting enzyme were differentially regulated in Px-UNx compared to sham (fig. 6B).

DISCUSSION

Here we characterized two preclinical rat models of DbCM and DN by superimposing isoprenaline treatment and UNx, respectively, on Px. Px led to marked alterations in glucose homeostasis and induced morphological and functional changes related to cardiovascular and renal endpoints. While no synergistic effect was revealed by superimposing the cardiac stressor, isoprenaline, to Px, superimposing UNx to Px in rats led to exacerbated DN as measured by alterations in albuminuria and GFR.

In agreement with previous findings [42], we demonstrated that 90%, but not 60%, Px induced permanent, stable hyperglycemia, concomitant with a surgically induced reduction in beta cell mass and thereby lower plasma insulin levels. Interestingly, we found that despite having undergone 90% Px, normoglycemia was restored three weeks after surgery in a subset (50%) of rats, termed non-responders, in experiment 1. These rats were able to maintain adequate insulin production to support normoglycemia. Hereafter, the Px procedure was further refined, which resulted in a reduction to 2% of non-responders in subsequent studies. Evidently, a certain threshold in critical beta cell mass exists.

Besides demonstrating a pronounced and sustained diabetic phenotype, including decreased C-peptide as well as increased HbA1c, the Px rat also exhibited mild cardiac hypertrophy and remodeling indicated by increased relative LV mass, LV wall thickness and LVIDd. Although EF was preserved, early systolic dysfunction was revealed by increased LVIDs. In DbCM, diastolic dysfunction is known to precede systolic dysfunction but, in this study, unfortunately,

several indices of diastolic function, including the late filling of the LV, could not be derived due to low temporal resolution and thus E/A fusion during the echocardiographic examination. Although the LV filling pattern could not be fully evaluated, the finding of a decreased early filling, corresponding to the peak E wave mitral inflow velocity, may be indicative of impaired relaxation and thus early diastolic dysfunction in Px rats. Furthermore, Px intervention altered the expression of selected genes involved in the pathogenesis of DbCM as suggested by the Diabetes Complications Consortium [16]. For instance, the major cardiac glucose transporter, GLUT4, was downregulated in Px. Interestingly, impaired insulin signaling, including decreased recruitment of GLUT4 to the plasma membrane, has been implicated in promoting cardiomyocyte stiffness in the diabetic heart [43]. In support of an attenuated contractile function, a shift from the 'fast' isoform α-MHC to the slower β-MHC along with decreased SERCA-2 expression was found in LV tissue.

An important advantage of the Px model is that it reflects the isolated effects of reduced beta cell mass, without the potential multiple-organ toxic effects of STZ [24] or the confounding effects of obesity and impaired leptin signaling found in e.g. ZDF rats. A disadvantage, however, is that not only beta cells, but also exocrine acinar cells are excised during 90% Px. The lack of pancreatic enzymes following Px [44] may thus act as a confounder by potentially inducing malnutrition and growth retardation. In future studies, supplementation with pancreatic enzymes may therefore be considered to avoid such potential effects.

Isoprenaline is a β-adrenergic agonist promoting cardiac hypertrophy, fibrosis, and systolic dysfunction in rats when administered in supraphysiological dosages [31,45,46]. In the present study, isoprenaline treatment *per se* did not induce cardiac hypertrophy or remodeling but did induce increased LV fibrosis and reduced systolic function. A possible explanation for the lack of isoprenaline-induced LV hypertrophy is that the cardiac remodeling may be reversible as indicated previously by Golomb *et al.* [47], demonstrating reversal just seven days after cessation of isoprenaline. In the present study, LV changes were assessed nearly four weeks after isoprenaline treatment and in comparison to previous studies where a single high-dose regimen has been used [30,45], a relatively low isoprenaline dosage was applied.

Unexpectedly, the combination of Px and isoprenaline treatment did not accentuate or accelerate LV morphological or functional changes. Clinical studies of patients with diabetes have previously shown an increased susceptibility to hemodynamic stressors [48,49] and we thus hypothesized that the cardiac changes induced by isoprenaline would be accelerated and

accentuated when superimposed on Px. Isoprenaline induced a nearly 30% mortality rate in sham-operated rats after the first exposure, whereas no isoprenaline-related deaths were observed in Px animals. Mortality following isoprenaline treatment has been reported previously using higher doses in non-diabetic rats [30,31,45]. In the present study, the expression of β_2-receptors was slightly downregulated by Px whilst PDE3A was upregulated, which could attenuate responsiveness to β-receptor stimulation by isoprenaline [50], and hence partly explain the lack of synergy, but also the increased mortality rate. Conversely, AC6, known to improve cardiac function and responsiveness to β-receptor stimulation [51], was upregulated by Px. Another explanation could be related to the decreased heart rate in Px rats. Lower heart rates will have longer refractory periods and this phenomenon could perhaps protect against isoprenaline-induced tachycardia and arrhythmias. However, further experiments are needed to elucidate this subject further.

UNx is known to accelerate DN progression in rodents [18]. Along this line, we observed that the combination of Px and UNx induced several hallmarks of DN. Px-UNx rats displayed profound renal and glomerular hypertrophy, which together with increased GFR are indicative of renal hyperfiltration. These phenomena are also observed in patients during the early phase of DN disease progression [52]. Importantly, Px-UNx animals presented with persistent albuminuria detectable as early as two weeks post-surgery. Similarly, urine NGAL excretion was increased, which is indicative of tubular damage and supported by increased RNA expression levels of the clinical biomarkers, NGAL and KIM-1 [53,54]. Urine sTNFR I and II excretion was increased; a finding that corresponds to reports of diabetic patients with diabetic kidney disease [55]. Finally, urine podocalyxin excretion was increased in line with observations of early podocyte injury in human patients [56].

Histopathological evaluation of kidneys from the Px-UNx model did not reveal evidence of renal fibrosis or glomerulosclerosis as measured by intra-glomerular type IV collagen. However, stereological assessment of the kidney revealed massive renal and glomerular hypertrophy. Together with the measured GFR, these data demonstrate that the Px-UNx rat represents a model of early stage DN in human patients. Longer term studies, beyond the ten weeks reported here, are likely required for progression of DN with resulting GFR loss, glomerulosclerosis, and tubulointerstitial fibrosis.

Although non-diabetic uninephrectomized animals were not included as a control in this study, our data suggest that UNx accelerates DN in the Px rat. Compared with Px rats from experiment

2, UNx-Px rats displayed augmented urine ACR in experiment 3. This suggests that kidney injury is accelerated in Px-UNx compared with Px alone.

CONCLUSION

In conclusion, 90% Px in the rat resulted in a robust model of experimental diabetes with a surgically-induced onset of hyperglycemia concomitant with hypoinsulinemia. The observation of increased LV wall thickness and internal diameters indicated that Px may mimic early stages of DbCM disease development. The preclinical applicability was supported by changes in expression levels in genes centrally involved in cardiomyocyte changes related to DbCM. However, the combination of isoprenaline and Px did not further accentuate DbCM development. Px in combination with UNx exhibited pronounced albuminuria, renal and glomerular hypertrophy together with increased GFR resembling features of early stage DN. The Px and the Px-UNx models could therefore be useful to study the potential efficacy of new therapeutic interventions for attenuating early disease progression in DbCM and DN, respectively.

ABBREVIATIONS

AC: adenylate cyclase
ACR: albumin creatinine ratio
ANOVA: analysis of variance
DbCM : diabetic cardiomyopathy
DN: diabetic nephropathy
EF: ejection fraction
FITC: fluorescein isothiocyanate
GFR: glomerular filtration rate
GLUT: glucose transporter
HbA1c: glycated hemoglobin
Iso: isoprenaline
KIM-1: Kidney Injury Molecule-1
LV: left ventricle
LVAWd: left ventricular anterior wall thickness in diastole
LVAWs: left ventricular anterior wall thickness in systole
LVIDd: left ventricular internal diameter in diastole
LVIDs: left ventricular internal diameter in systole
LVPWd: left ventricular posterior wall thickness in diastole
LVPWs: left ventricular posterior wall thickness in systole
MHC: myosin heavy chain

NGAL: neutrophil gelatinase-associated lipocalin
OGTT: oral glucose tolerance test
PAS: periodic acid-Schiff
PDE3A: phosphodiesterase 3A
Px: pancreatectomy
SEM: standard error of mean
SERCA: sarco/endoplasmic reticulum Ca^{2+}-ATPase
sTNFR: soluble tumor necrosis factor receptor
STZ: streptozotocin
UNx: uninephrectomy
UCP: uncoupling protein
ZDF rat: Zucker diabetic fatty rat

DECLARATIONS

Ethics approval and consent to participate

The animal experiments were approved by The Danish Animal Experiments Inspectorate (license no. 2019-15-0201-01648, 2017-15-0201-01183, 2017-15-0201-01286) and conformed to the European Parliament Directive on the Protection of Animals Used for Scientific Purposes (2010/63/EU).

Consent for publication

All authors have declared their consent for this publication.

Availability of data and materials

All data and materials are available upon request.

Competing interests

LT, MVO, AAP, PJP, LNF, TSe, STT, JJ, NEZ are employed by Gubra.

Funding

The salary of LT is partly funded by Innovation Fund Denmark (grant no: 7038-00070B). RTL received a PhD studentship from the British Heart Foundation (grant no: FS/14/59/31282).

Authors' Contribution

Conception and design of research: MVO, LNF, TSk, JJ, NEZ.
Acquisition of data: LT, MVO, AAP, PJP, RTL, TSe, TJJ, NEZ.
Analysis and interpretation the data: LT, MVO, PJP, AJM, LNF, TXP, TSe, TJJ, STT, TSk, JJ, MBT, NEZ.
Wrote the manuscript: LT, MVO, JJ, NEZ.

All authors read and approved the final manuscript.

Acknowledgements
The authors would like to acknowledge the skilled assistance of Camilla Malec and Helene Dyhr who performed the pancreatectomy and uninephrectomy surgeries.

Authors' information
Not applicable

REFERENCES

1. International Diabetes Federation. IDF Diabetes Atlas - 2019. 9th editio. Brussels, Belgium; 2019.

2. AD. Deshpande, M. Harris-Hayes MS. Epidemiology of diabetes and diabetes-related complications. Phys Ther. 2008;88:1254–1264.

3. Secrest AM, Washington RE, Orchard TJ. Chapter 35: Mortality in Type 1 Diabetes. Diabetes Am. 2014. p. 1–16.

4. Bell DSH. Heart failure: The frequent, forgotten, and often fatal complication of diabetes. Diabetes Care. 2003;26:2433–41.

5. Beckman JA, Paneni F, Cosentino F, Creager MA. Diabetes and vascular disease: Pathophysiology, clinical consequences, and medical therapy: Part II. Eur Heart J. 2013;34:2444–56.

6. Singh GM, Danaei G, Farzadfar F, Stevens GA, Woodward M, Wormser D, et al. The age-specific quantitative effects of metabolic risk factors on cardiovascular diseases and diabetes: A pooled analysis. PLoS One. 2013;8.

7. Boudina S. Clinical manifestations of diabetic cardiomyopathy. Hear Metab. 2009;45:10–4.

8. Rubler S, Dlugash J, Yuceoglu YZ, Kumral T, Branwood AW, Grishman A. New type of cardiomyopathy associated with diabetic glomerulosclerosis. Am J Cardiol. 1972;30:595–602.

9. Schannwell CM, Schneppenheim M, Perings S, Plehn G, Strauer BE. Left ventricular diastolic dysfunction as an early manifestation of diabetic cardiomyopathy. Cardiology. 2002;98:33–9.

10. Shimizu M, Umeda K, Sugihara N, Yoshio H, Ino H, Takeda R, et al. Collagen remodelling in myocardia of patients with diabetes. J Clin Pathol. 1993;46:32–6.

11. Hayat SA, Patel B, Khattar RS, Malik RA. Diabetic cardiomyopathy: Mechanisms, diagnosis and treatment. Clin Sci. 2004;107:539–57.

12. Betz B, Conway BR. Recent advances in animal models of diabetic nephropathy. Nephron - Exp Nephrol. 2014;126:191–5.

13. Rudberg S, Osterby R. Decreasing glomerular filtration rate - An indicator of more advanced diabetic glomerulopathy in the early course of microalbuminuria in IDDM adolescents? Nephrol Dial Transplant. 1997;12:1149–54.

14. Mauer SM, Lane P, Zhu D, Fioretto P SM. Renal structure and function in insulin-dependent diabetes mellitus in man. J Hypertens Suppl. 1992;10:17–20.

15. Breyer MD, Böttinger E, Brosius FC, Coffman TM, Harris RC, Heilig CW, et al. Mouse models of diabetic nephropathy. J Am Soc Nephrol. 2005;16:27–45.

16. AMDCC. Validation of Models of Cardiovascular Disease in Diabetes. Animal Models of Diabetic Complications Consortium; 2003. p. 1–13.

17. AMDCC. Validation of Mouse Models of Diabetic Nephropathy. Animal Models of Diabetic Complications Consortium; 2003. p. 1–12.

18. Nickerson HD, Dutta S. Diabetic complications: Current challenges and opportunities. J Cardiovasc Transl Res. 2012;5:375–9.

19. Miric G, Dallemagne C, Endre Z, Margolin S, Taylor SM, Brown L. Reversal of cardiac and renal fibrosis by pirfenidone and spironolactone in streptozotocin-diabetic rats. Br J Pharmacol. 2001;133:687–94.

20. Katoh M, Ohmachi Y, Kurosawa Y, Yoneda H, Tanaka N, Narita H. Effects of imidapril and captopril on streptozotocin-induced diabetic nephropathy in mice. Eur J Pharmacol. 2000;398:381–7.

21. Fernandes SM, Mendes Cordeiro P, Watanabe M, Dezoti Da Fonseca C, De M, Fernandes Vattimo F. The role of oxidative stress in streptozotocin-induced diabetic nephropathy in rats. Arch Endocrinol Metab. 2016;60.

22. Sembach FE, Fink LN, Johansen T, Boland BB, Secher T, Thrane ST, et al. Impact of sex on diabetic nephropathy and the renal transcriptome in UNx db/db C57BLKS mice. Physiol Rep. NLM (Medline); 2019;7:e14333.

23. Arow M, Waldman M, Yadin D, Nudelman V, Shainberg A, Abraham NG, et al. Sodium-glucose cotransporter 2 inhibitor Dapagliflozin attenuates diabetic cardiomyopathy. Cardiovasc Diabetol. 2020;19.

24. Bolzán AD, Bianchi MS. Genotoxicity of Streptozotocin. Diabetes. 2002;512:579–82.

25. Camacho P, Fan H, Liu Z, He J-Q. Small mammalian animal models of heart disease. Am J Cardiovasc Dis. 2016.

26. Bugger H, Abel ED. Rodent models of diabetic cardiomyopathy. Dis Model Mech. 2009;2:454–66.

27. Eulálio JMR, Bon-Habib ACC, de Oliveira Soares D, Corrêa PGA, Pineschi GPF, Diniz VS, et al. Critical analysis and systematization of rat pancreatectomy terminology. Acta Cir Bras. 2016;31:698–704.

28. Tanigawa K, Nakamura S, Kawaguchi M, Xu G, Kin S, Tamura K. Effect of aging on B-cell function and replication in rat pancreas after 90% pancreatectomy. Pancreas. 1997;15:53–9.

29. Hoit BD, Castro C, Bultron G, Knight S, Matlib MA. Noninvasive evaluation of cardiac

dysfunction by echocardiography in streptozotocin-induced diabetic rats. J Card Fail. 1999;5:324–33.

30. Grimm D, Elsner D, Schunkert H, Pfeifer M, Griese D, Bruckschlegel G, et al. Development of heart failure following isoproterenol administration in the rat: Role of the renin-angiotensin system. Cardiovasc Res. 1998;37:91–100.

31. Leenen FHH, White R, Yuan B. Isoproterenol-induced cardiac hypertrophy: Role of circulatory versus cardiac renin-angiotensin system. Am J Physiol - Hear Circ Physiol. 2001;281:2410–6.

32. Zheng S, Huang Y, Yang L, Chen T, Xu J, Epstein PN. Uninephrectomy of Diabetic OVE26 Mice Greatly Accelerates Albuminuria, Fibrosis, Inflammatory Cell Infiltration and Changes in Gene Expression. Nephron - Exp Nephrol. 2011;119.

33. Uil M, Scantlebery AML, Butter LM, Larsen WB, De Boer OJ, Leemans JC, et al. Combining streptozotocin and unilateral nephrectomy is an effective method for inducing experimental diabetic nephropathy in the “resistant” C57Bl/6J mouse strain OPEN. Sci Rep. 2018;8.

34. Goldstein SA, Evangelista A, Abbara S, Arai A, Asch FM, Badano LP, et al. Multimodality imaging of diseases of the thoracic aorta in adults: From the American society of echocardiography and the european association of cardiovascular imaging: Endorsed by the society of cardiovascular computed tomography and society for cardiova. J Am Soc Echocardiogr. 2015;28:119–82.

35. Teichholz LE, Herman V, Kreulen T, Gorlin R. Problems in Echocardiographic Presence or Absence Volume Determinations : Correlations in the of Asynergy. Am J Cardiol. 1976;37:7–11.

36. Rieg T. A high-throughput method for measurement of glomerular filtration rate in conscious mice. J Vis Exp. 2013;1–6.

37. Paulsen SJ, Vrang N, Larsen LK, Larsen PJ, Jelsing J. Stereological assessment of pancreatic beta-cell mass development in male Zucker Diabetic Fatty (ZDF) rats: correlation with pancreatic beta-cell function.

38. Paulsen SJ, Vrang N, Larsen LK, Larsen PJ, Jelsing J. Stereological assessment of pancreatic beta-cell mass development in male Zucker Diabetic Fatty (ZDF) rats: Correlation with pancreatic beta-cell function. J Anat. 2010;217:624–30.

39. Cullen-Mcewen LA, Armitage JA, Nyengaard JR, Bertram JF. Estimating nephron number in the developing kidney using the physical disector/fractionator combination. Methods Mol Biol. Humana Press Inc.; 2012;886:109–19.

40. Dobin A, Davis CA, Schlesinger F, Drenkow J, Zaleski C, Jha S, et al. STAR: Ultrafast universal RNA-seq aligner. Bioinformatics. 2013;29:15–21.

41. Love MI, Huber W, Anders S. Moderated estimation of fold change and dispersion for RNA-seq

data with DESeq2. Genome Biol. 2014;15:1–21.

42. Liu YQ, Nevin PW, Leahy JL. β-Cell adaptation in 60% pancreatectomy rats that preserves normoinsulinemia and normoglycemia. Am J Physiol - Endocrinol Metab. 2000;279:68–73.

43. Jia G, Demarco VG, Sowers JR. Insulin resistance and hyperinsulinaemia in diabetic cardiomyopathy HHS Public Access. Nat Rev Endocrinol. 2016;12:144–53.

44. Hotz J, Oberna RG, Clodi PH. Reserve Capacity of the Exocrine Pancreas Enzyme Secretion and Fecal Fat Assimilation in the 95% Pancrcatectomized Rat.

45. Králová E, Mokrán T, Murín J, Stankovicová T. Electrocardiography in two models of isoproterenol-induced left ventricular remodeling. Physiol Res. 2008;57 Suppl 2.

46. Benjamin IJ, Jalil JE, Tan LB, Cho K, Weber KT, Clark WA. Isoproterenol-induced myocardial fibrosis in relation to myocyte necrosis. Circ Res. 1989;65:657–70.

47. Golomb E, Abassi ZA, Cuda G, Stylianou M, Panchal VR, Trachewsky D, et al. Angiotensin II maintains, but does not mediate, isoproterenol-induced cardiac hypertrophy in rats. Am J Physiol - Hear Circ Physiol. 1994;267.

48. Haffner SM, Lehto S, Rönnemaa T, Pyörälä K, Laakso M. Mortality from coronary heart disease in subjects with type 2 diabetes and in nondiabetic subjects with and without prior myocardial infarction. N Engl J Med. 1998;339:229–34.

49. Fazel R, Fang J, Kline-Rogers E, Smith DE. Prognostic value of elevated biomarkers in diabetic and non-diabetic patients admitted for acute coronary syndromes. Heart. 91:388–90.

50. Wu H, Lee J, Vincent LG, Wang Q, Gu M, Lan F, et al. Epigenetic Regulation of Phosphodiesterases 2A and 3A Underlies Compromised β-Adrenergic Signaling in an iPSC Model of Dilated Cardiomyopathy. Cell Stem Cell. 2015;17:89–100.

51. Roth DM, Mei ;, Gao H, Lai ; N Chin, Drumm J, Dalton N, et al. Cardiac-Directed Adenylyl Cyclase Expression Improves Heart Function in Murine Cardiomyopathy. Circ J. 1999;99:3099–102.

52. Tonneijck L, Muskiet MHA, Smits MM, Van Bommel EJ, Heerspink HJL, Van Raalte DH, et al. Glomerular hyperfiltration in diabetes: Mechanisms, clinical significance, and treatment. J. Am. Soc. Nephrol. American Society of Nephrology; 2017. p. 1023–39.

53. Han WK, Bailly V, Abichandani R, Thadhani R, Bonventre J V. Kidney Injury Molecule-1 (KIM-1): A novel biomarker for human renal proximal tubule injury. Kidney Int. 2002;62:237–44.

54. Devarajan P. Neutrophil gelatinase-associated lipocalin (NGAL): A new marker of kidney disease. Scand J Clin Lab Invest. 2008. p. 89–94.

55. Carlsson AC, Östgren CJ, Nystrom FH, Länne T, Jennersjö P, Larsson A, et al. Association of soluble tumor necrosis factor receptors 1 and 2 with nephropathy, cardiovascular events, and total mortality in type 2 diabetes Open Access. Cardiovasc Diabetol. 2016;15:40.

56. Hara M, Yamagata K, Tomino Y, Saito A, Hirayama Y, Ogasawara S, et al. Urinary podocalyxin is an early marker for podocyte injury in patients with diabetes: Establishment of a highly sensitive ELISA to detect urinary podocalyxin. Diabetologia. 2012;55:2913–9.

FIGURES

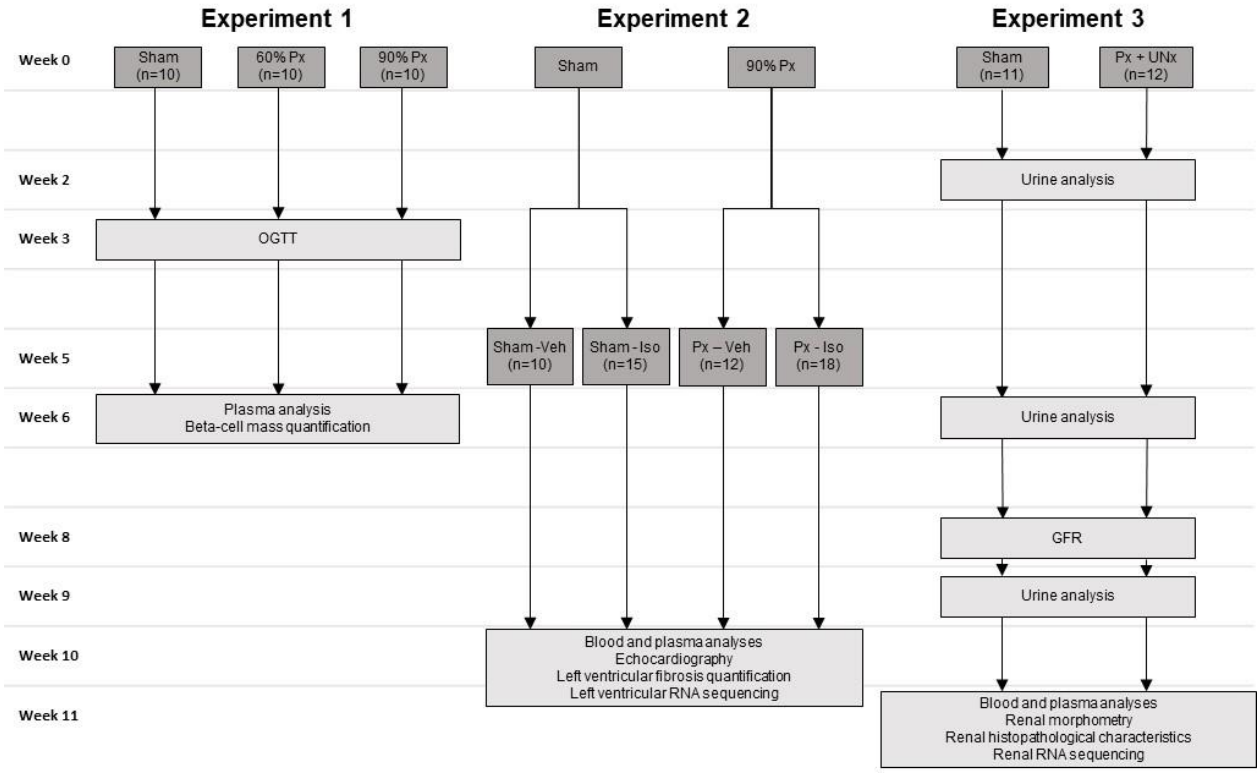

Figure 1. Study design of experiment 1-3. GFR: glomerular filtration rate, Iso: isoprenaline, OGTT: oral glucose tolerance test, Px: pancreatectomy, Veh: vehicle, UNx: uninephrectomy.

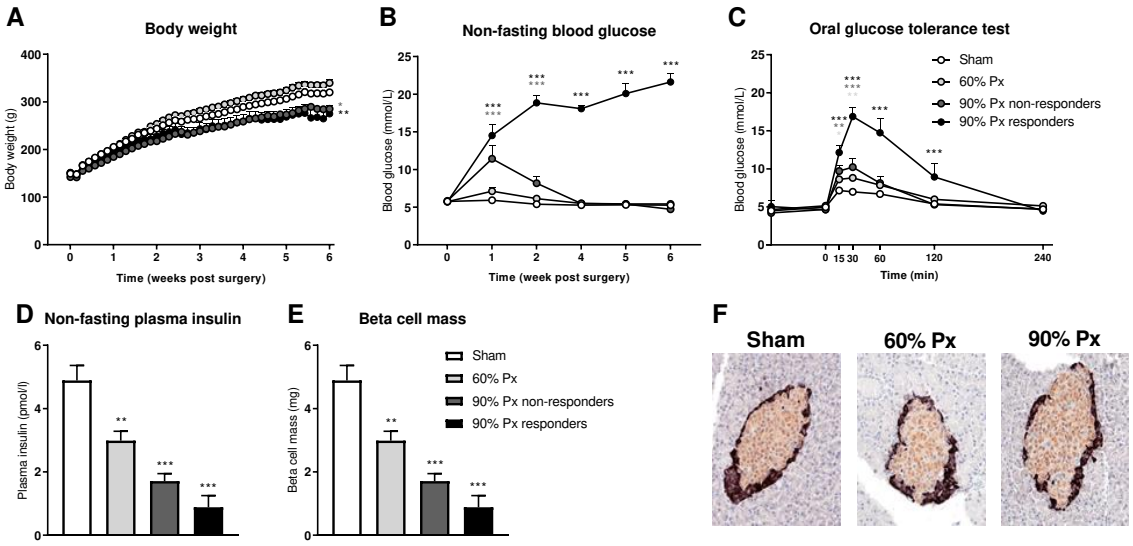

Figure 2. Body weight, blood glucose, plasma insulin, and beta cell mass for pancreatectomized animals. Body weight (A) and non-fasting blood glucose (B) measured in rats subjected to pancreatectomy (Px), where either 60% Px or 90% Px was removed, or sham surgery throughout the study period. Blood glucose levels from an oral glucose tolerance test performed three weeks after surgery (C). Non-fasting plasma insulin and total beta-cell mass determined by stereology six weeks after surgery (D-E) and representative images of sections from sham and Px rats stained for beta cells (orange-brown; insulin-immunoreactive) and non-beta cells (black; pancreatic polypeptide, somatostatin and glucagon-immunoreactive) (F). Data is presented as mean + SEM. n=10,10,5,5. Two-way ANOVA with Bonferroni's post-hoc test was applied to blood glucose data and one-way ANOVA with Tukey's post-hoc test to insulin and beta cell mass data. *p<0.05, **p<0.01, ***p<0.001 vs Sham.

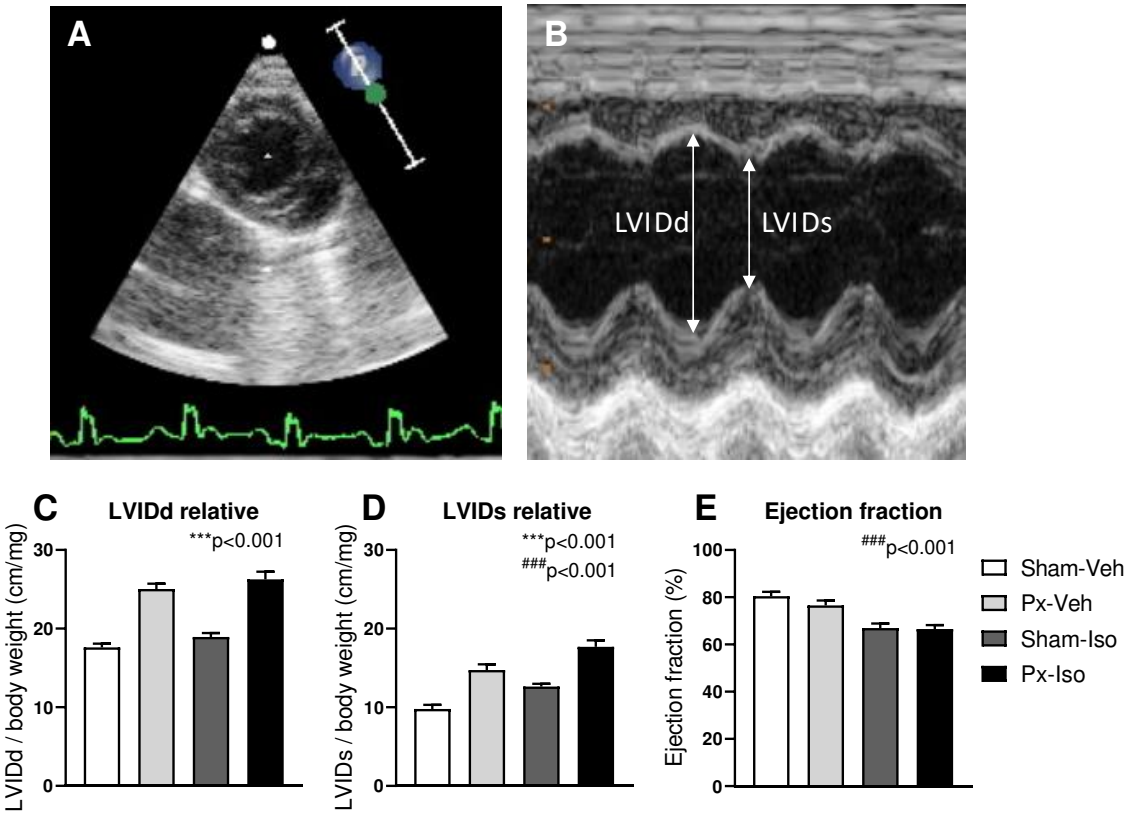

Figure 3. Echocardiographic assessment of left ventricular morphology and function in pancreatectomized and isoprenaline treated rats. Echocardiographic parasternal short-axis views (A) were used to obtain M-mode images at the level of the papillary muscles (B) Left ventricular (LV) end-diastolic and -systolic diameters (LVIDd, LVIDs) normalized to body weight (C-D) and ejection fraction (E) were evaluated ten weeks after sham surgery or pancreatectomy (Px) in vehicle (Veh)- or isoprenaline (Iso) treated rats. Data is presented as mean + SEM. n=10,15,12,18. Two-way ANOVA; main effect of pancreatectomy ***p<0.001, main effect of isoprenaline treatment $^{###}$p<0.001.

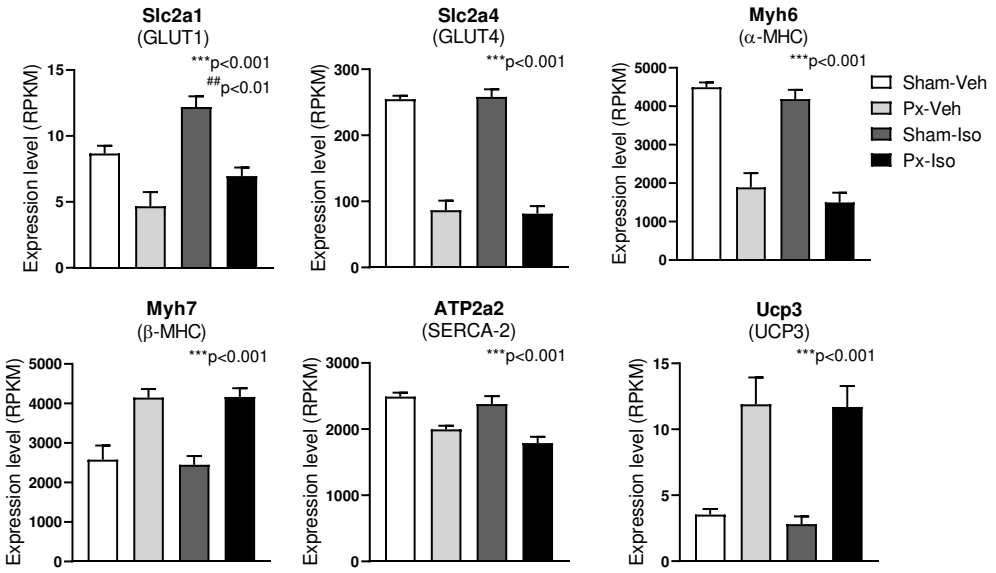

Figure 4. Expression of selected genes in the left ventricle of pancreatectomized and isoprenaline treated rats. Expression levels of genes relevant for cardiac function ten weeks after sham surgery or 90% pancreatectomy (Px) in vehicle (Veh)- or isoprenaline (Iso) treated rats. Data is presented as mean + SEM. n=7,8,8,8. Two-way ANOVA; main effect of pancreatectomy ***p<0.001, main effect of isoprenaline treatment $^{\#\#}$p<0.01. GLUT: glucose transporter, MHC: myosin heavy chain. SERCA: sarco/endoplasmic reticulum $Ca2^{+}$-ATPase, UCP: Uncoupling protein.

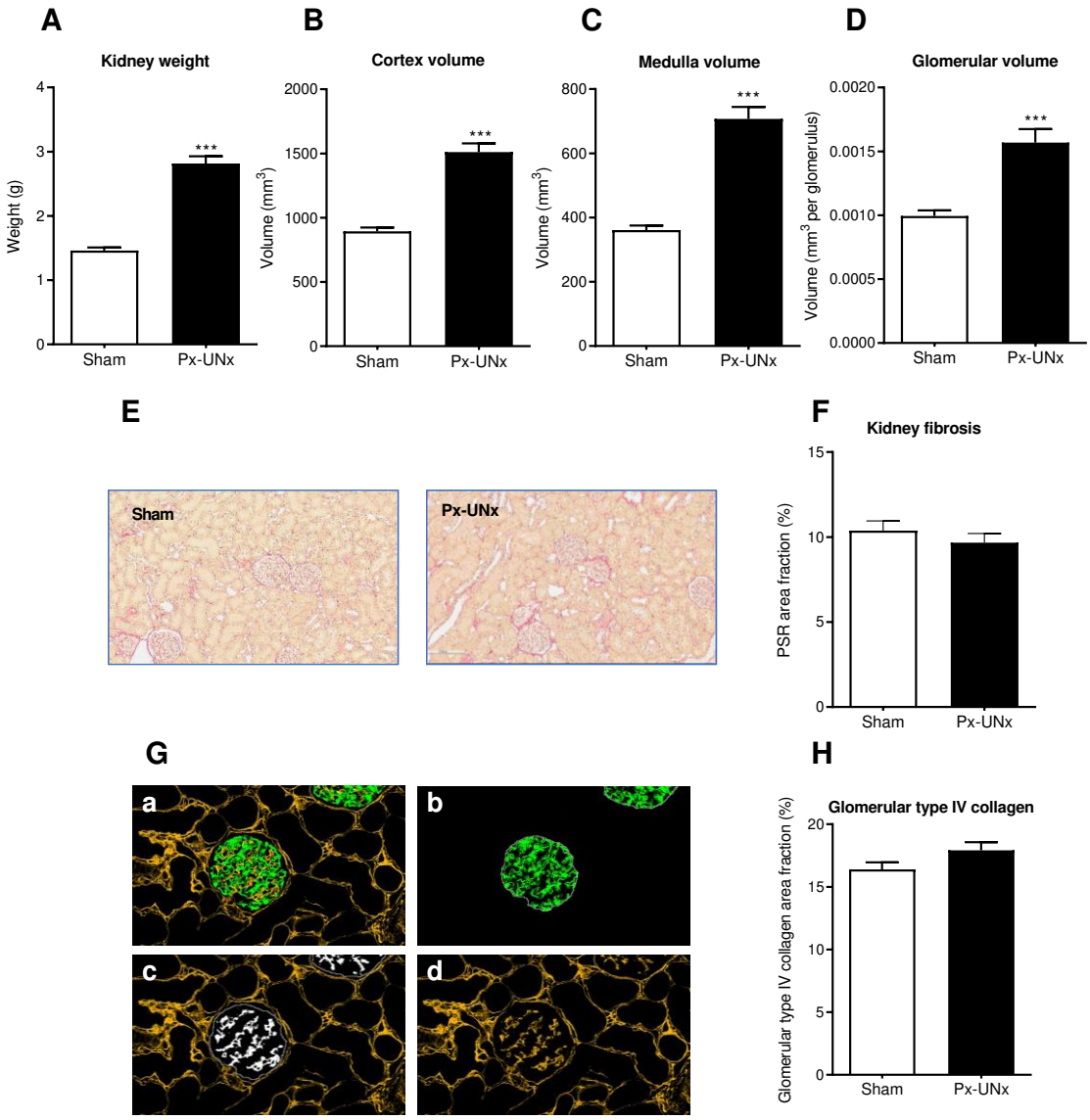

Figure 5. Renal morphometric and histopathological characteristics in pancreatectomized-uninephrectomized rats. Measurements were performed eleven weeks after sham or pancreatectomy-uninephrectomy (Px-UNx). Kidney weight and volume of renal compartments (A-D). Representative images of Picro Sirius Red (PSR) stained kidney sections and total renal fibrosis quantification (E-F). Representative images of kidney sections stained for co-localization type IV collagen (yellow) and podocin (green), and quantification of intra-glomerular type IV collagen (white) (G-H). Data is presented as mean + SEM. n=11-12 in each group. Unpaired t-test; ***p<0.001 vs. sham.

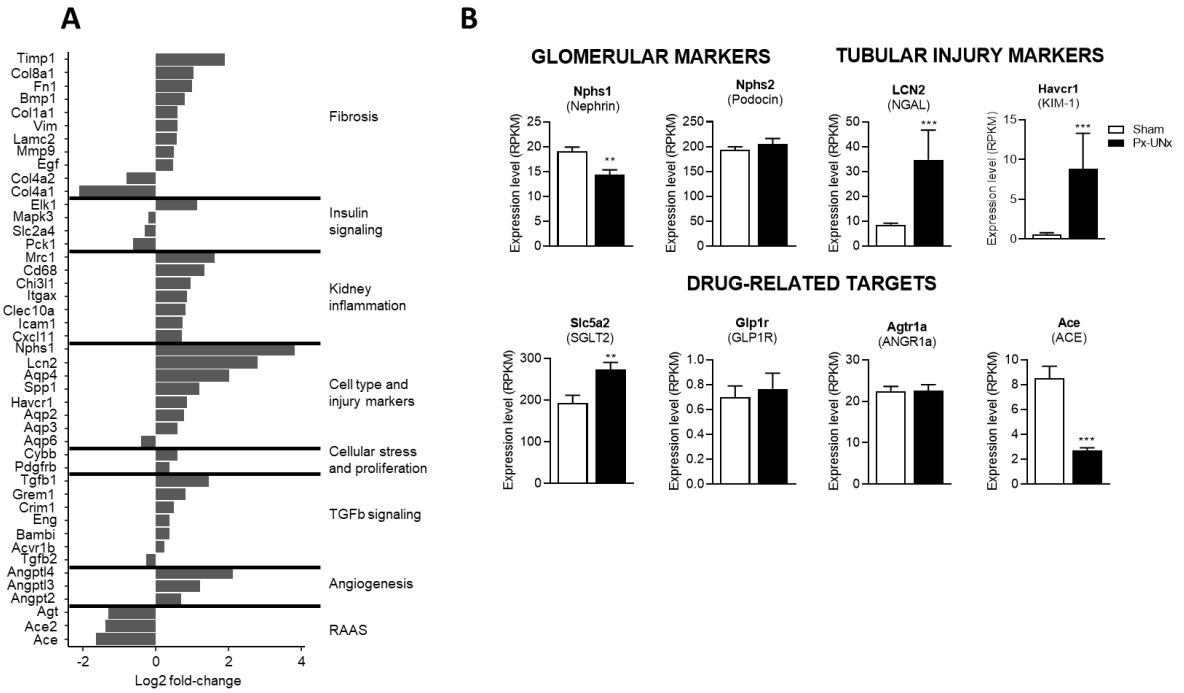

Figure 6. Renal gene expression in pancreatectomized-uninephrectomized rats. Measurements were performed at termination, eleven weeks after sham or pancreatectomy-uninephrectomy (Px-UNx). Pathway summary presenting selected genes that are significantly regulated in the renal cortex of Px-UNx vs. Sham animals at $p<0.01$ significance level (A). Expression levels of selected genes in the renal cortex (B). Data are mean + SEM (n=11-12). Unpaired t-test; **p<0.01, **p<0.001 vs Sham after correction for gene-wise multiple testing. ACE: Angiotensin I converting enzyme, ANGR1a: Angiotensin II receptor, type 1a, GLP1R: Glucagon-like peptide 1 receptor, KIM-1: kidney injury molecule 1, NGAL: neutrophil gelatinase-associated lipocalin, RAAS: renin-angiotensin-aldosterone system, SGLT2: Sodium-glucose transport protein 2.

TABLES

Table 1. Body weight, plasma markers, left ventricular mass, and collagen in pancreatectomized and isoprenaline treated rats. Measurements were performed at pre-surgery and/or ten weeks after sham surgery or pancreatectomy (Px) in vehicle (Veh)- or isoprenaline (Iso) treated rats. Data is presented as mean ± SEM. Two-way ANOVA; main effect of pancreatectomy *p<0.05, ***p<0.001, main effect of isoprenaline treatment ###p<0.001.

	Sham-Veh (n=10)	**Px-Veh** (n=15)	**Sham-Iso** (n=12)	**Px-Iso** (n=18)	**Main effect**
Body weight (g, pre-surgery)	249 ± 5	253 ± 3	247 ± 6	248 ± 3	ns.
Body weight (g, week 10)	454 ± 10	293 ± 11	447 ± 12	297 ± 10	***
Blood glucose (mmol/L, pre-surgery)	3.3 ± 0.2	3.6 ± 0.2	3.4 ± 0.1	3.4 ± 0.1	ns
Blood glucose (mmol/L, week 10)	4.8 ± 0.1	24.7 ± 1.0	4.7 ± 0.2	22.4 ± 1.5	***
Plasma insulin (pg/mL, week 10)	835 ± 96	180 ± 25	755 ± 87	173 ± 23	***
C-peptide (pg/mL, week 10)	2805 ± 105	839 ± 110	3012 ± 198	697 ± 70	***
HbA1c (%, week 10)	3.8 ± 0.1	9.2 ± 0.4	4.3 ± 0.5	10.0 ± 0.2	***
Left ventricular mass (mg, week 10)	966 ± 48	725 ± 30	1020 ± 36	760 ± 37	*
Left ventricular collagen area fraction (%, week 10)	3.7 ± 0.4	3.1 ± 0.2	7.6 ± 0.6	6.28 ± 0.5	* ###

Table 2. Echocardiographic assessment of left ventricular morphology and function in pancreatectomized and isoprenaline treated rats. Left ventricular wall thickness, filling parameters and heart rate ten weeks after sham surgery or pancreatectomy (Px) in vehicle (Veh)- or isoprenaline (Iso) treated rats. Heart rate was measured during echocardiography in week ten. Data is presented as mean ± SEM. Two-way ANOVA; main effect of pancreatectomy **p<0.01, ***p<0.001, main effect of isoprenaline treatment $^{\#}$p<0.05.

	Sham-Veh (n= 10)	**Px-Veh** (n=15)	**Sham-Iso** (n=12)	**Px-Iso** (n=18)	**Main effect**
Relative LVAWd (mm/mg BW)	3.5 ± 0.3	5.1 ± 0.4	3.6 ± 0.2	4.8 ± 0.3	***
Relative LVPWd (mm/mg BW)	3.3 ± 0.3	4.4 ± 0.2	3.1 ± 0.2	4.2 ± 0.2	***
Relative LVAWs (mm/mg BW)	6.3 ± 0.3	8.9 ± 0.5	5.9 ± 0.3	7.6 ± 0.4	*** #
Relative LVPWs (mm/mg BW)	5.7 ± 0.4	6.9 ± 0.3	4.6 ± 0.3	6.3 ± 0.3	*** #
Peak E wave velocity (cm/s)	114 ± 3	107 ± 4	123 ± 5	104 ± 4	**
Deceleration time (ms)	42 ± 2	47 ± 5	41 ± 3	42 ± 3	ns.
Heart rate (bpm)	368 ± 3	299 ± 8	373 ± 3	281 ± 18	***

Table 3. Urine markers in pancreatectomized-uninephrectomized and sham rats. Measurements were performed after two, six, and nine weeks in sham operated or pancreatectomized-uninephrectomized (Px-UNx) rats. Data is presented as mean ± SEM. Two-way repeated measures ANOVA with Bonferroni's Multiple Comparisons post-hoc test; **p<0.01, ***p<0.001 vs. Sham.

	Week 2			Week 6			Week 9		
	Sham (n=12)	**Px-UNx** (n=11)		**Sham** (n=12)	**Px-UNx** (n=11)		**Sham** (n=12)	**Px-UNx** (n=11)	
Creatinine (µmol/L)	7197 ± 661	993 ± 209	***	8189 ± 444	606 ± 85	***	8273 ± 445	520 ± 65	***
Albumin-to-creatinine (µg/mg)	109 ± 13	1250 ± 653	***	207 ± 60	10281 ± 6239	***	370 ± 170	13473 ± 7619	***
NGAL-to-creatinine (µg/mg)	3.27 ± 0.8	16.6 ± 2.2	***	3.84 ± 0.4	14.9 ± 1.7	***	2.69 ± 0.4	13.3 ± 1.9	***
Podocalyxin-to-creatinine (µg/mg)	19.9 ± 2.7	76.2 ± 9.3		14.6 ± 1.8	186.9 ± 59.3	***	11.8 ± 2.0	195.2 ± 41.9	***
sTNFR-I- to-creatinine (pg/mg)	36.0 ± 3.4	259 ± 32		23.6 ± 1.4	427 ± 117	***	21.3 ± 1.3	447 ± 133	***
sTNFR-II-to-creatinine (pg/mg)	2521 ± 197	5212 ± 413	***	1460 ± 122	3520 ± 391	***	1348 ± 163	2743 ± 414	**

Table 4. Plasma markers and glomerular filtration rate in pancreatectomized-uninephrectomized rats. Blood and plasma levels at eleven weeks in sham operated or pancreatectomized-uninephrectomized (Px-UNx) rats. Glomerular filtration rate was measured eight weeks after surgery. Data are presented as mean ± SEM. Unpaired t-test; *p<0.05, **p<0.01, ***p<0.001 vs. Sham.

	Sham (n=12)	**Px-UNx** (n=11)	
Blood glucose (mmol/L)	4.8±0.1	26.2±1.8	***
Insulin (pg/mL)	782±102	193±58	***
Urea (mmol/L)	5.5±0.2	9.4±0.7	***
Creatinine (µmol/L)	23.5±0.6	21.2±0.7	*
Cystatin C (ng/mL)	2373±50	2370±56	ns.
Glomerular filtration rate (ml/min/kg)	6.6±0.3	8.2±0.3	**

Figures

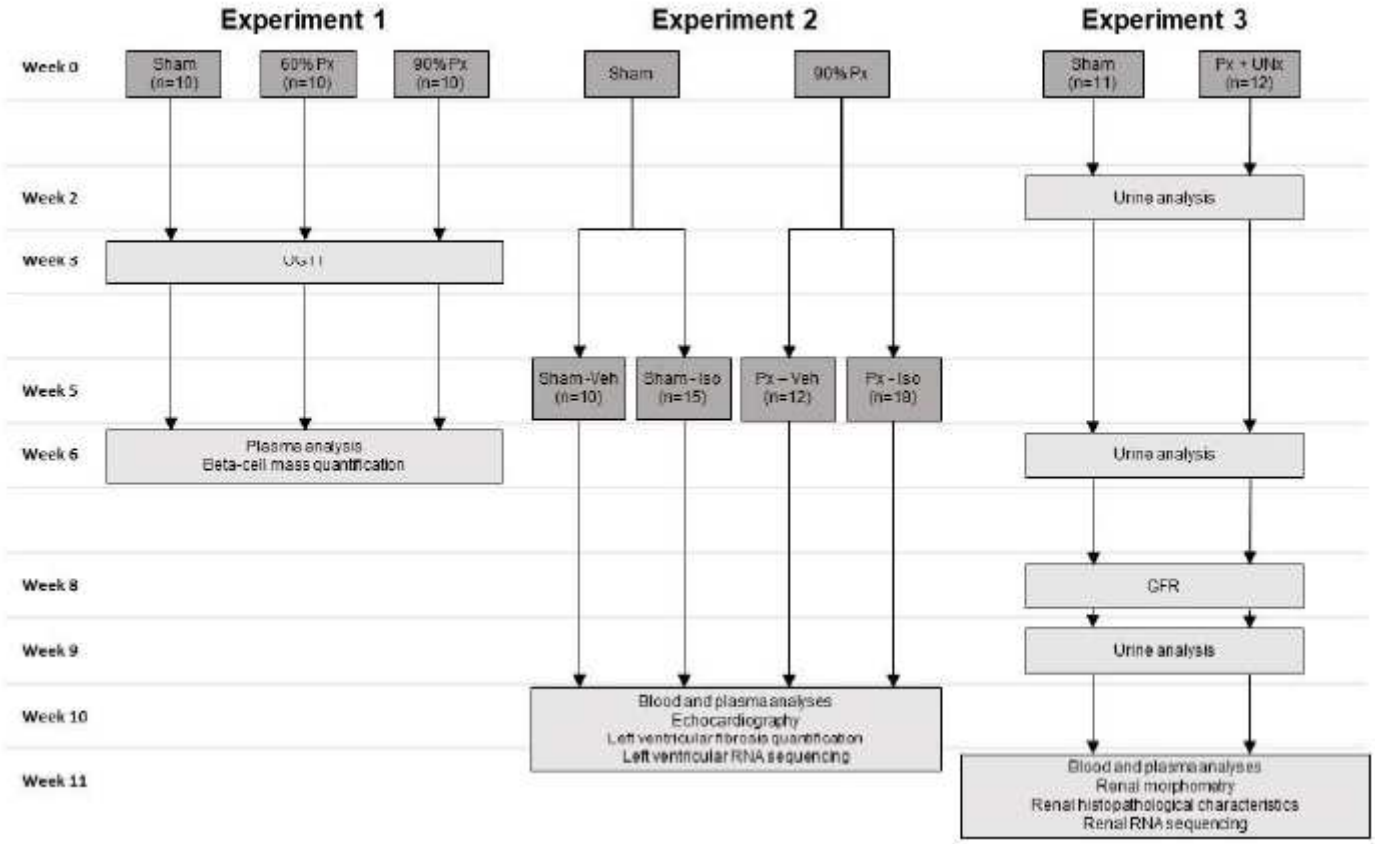

Figure 1

Study design of experiment 1-3. GFR: glomerular filtration rate, Iso: isoprenaline, OGTT: oral glucose tolerance test, Px: pancreatectomy, Veh: vehicle, UNx: uninephrectomy.

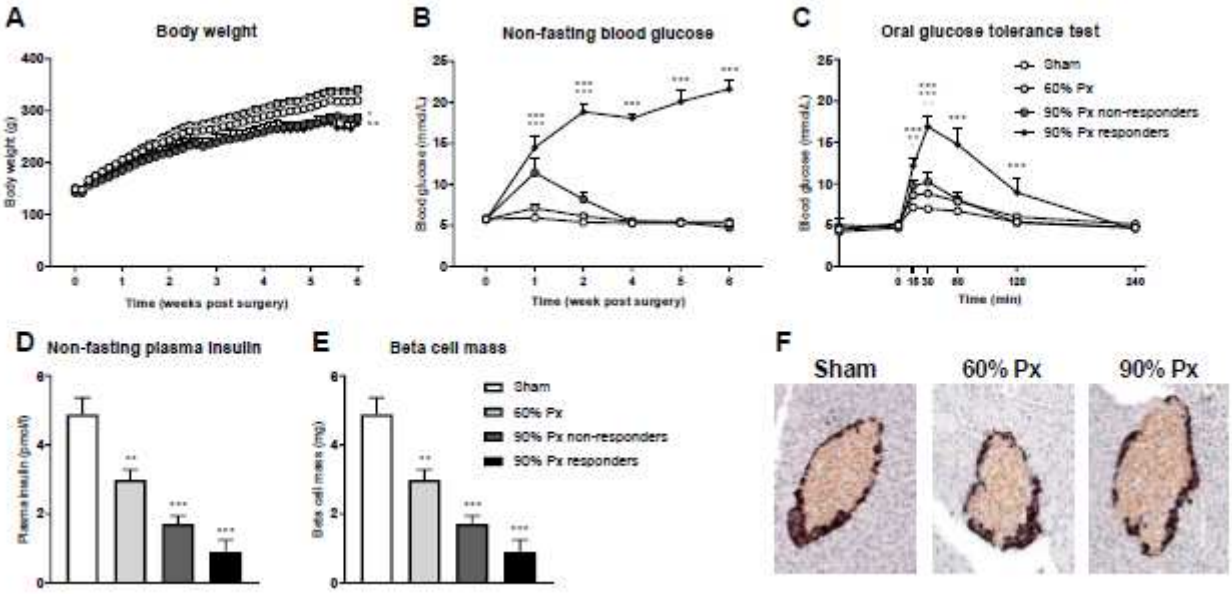

Figure 2

Body weight, blood glucose, plasma insulin, and beta cell mass for pancreatectomized animals. Body weight (A) and non-fasting blood glucose (B) measured in rats subjected to pancreatectomy (Px), where either 60% Px or 90% Px was removed, or sham surgery throughout the study period. Blood glucose levels from an oral glucose tolerance test performed three weeks after surgery (C). Non-fasting plasma insulin and total beta-cell mass determined by stereology six weeks after surgery (D-E) and representative images of sections from sham and Px rats stained for beta cells (orange-brown; insulin-immunoreactive) and non-beta cells (black; pancreatic polypeptide, somatostatin and glucagon-immunoreactive) (F). Data is presented as mean + SEM. n=10,10,5,5. Two-way ANOVA with Bonferroni's post-hoc test was applied to blood glucose data and one-way ANOVA with Tukey's post-hoc test to insulin and beta cell mass data. *p<0.05, **p<0.01, ***p<0.001 vs Sham.

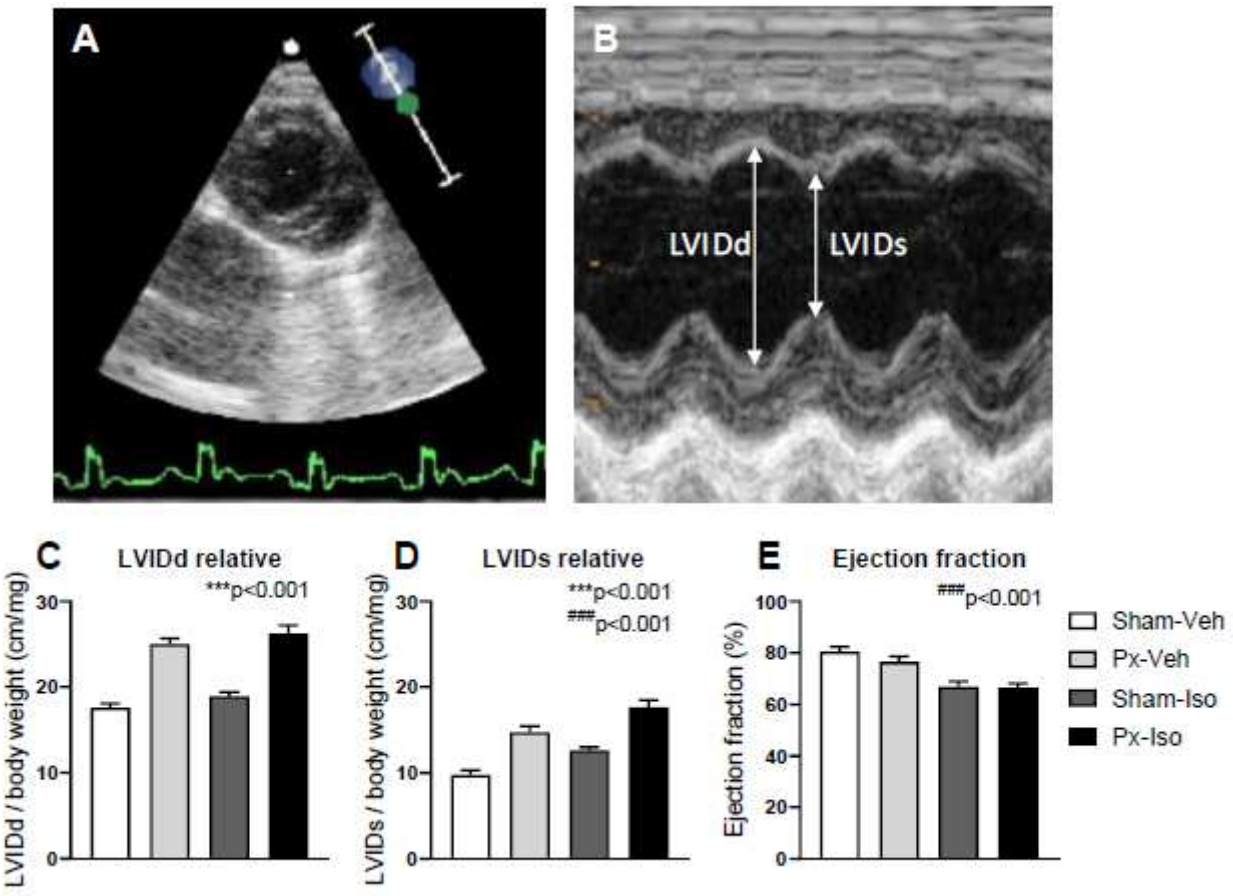

Figure 3

Echocardiographic assessment of left ventricular morphology and function in pancreatectomized and isoprenaline treated rats. Echocardiographic parasternal short-axis views (A) were used to obtain M-mode images at the level of the papillary muscles (B) Left ventricular (LV) end-diastolic and -systolic diameters (LVIDd, LVIDs) normalized to body weight (C-D) and ejection fraction (E) were evaluated ten weeks after sham surgery or pancreatectomy (Px) in vehicle (Veh)- or isoprenaline (Iso) treated rats. Data is presented

as mean + SEM. n=10,15,12,18. Two-way ANOVA; main effect of pancreatectomy ***p<0.001, main effect of isoprenaline treatment ###p<0.001.

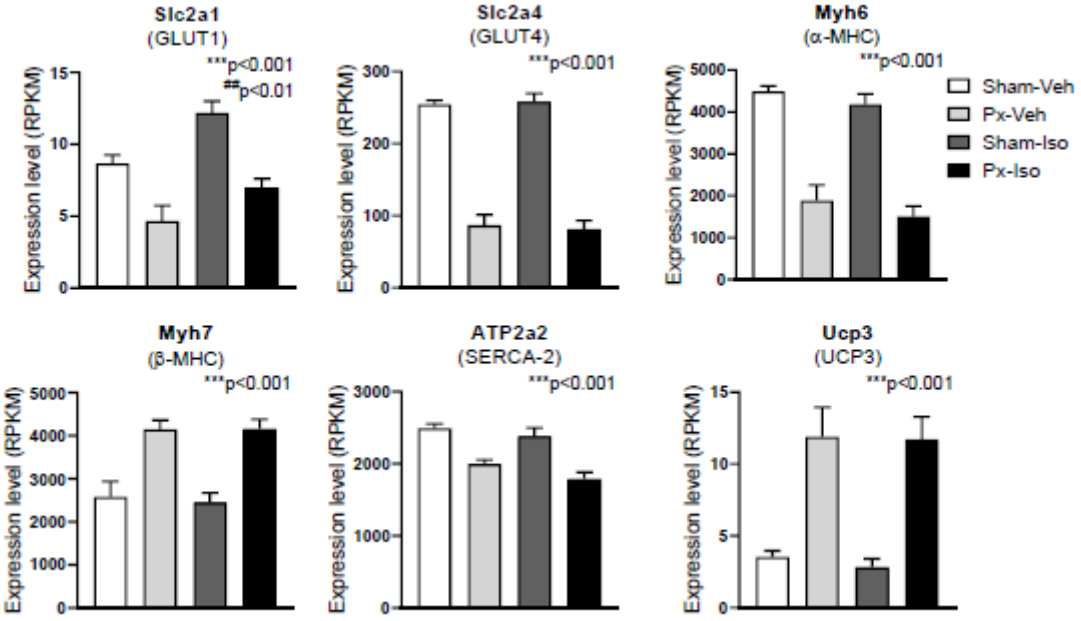

Figure 4

Expression of selected genes in the left ventricle of pancreatectomized and isoprenaline treated rats. Expression levels of genes relevant for cardiac function ten weeks after sham surgery or 90% pancreatectomy (Px) in vehicle (Veh)- or isoprenaline (Iso) treated rats. Data is presented as mean + SEM. n=7,8,8,8. Two-way ANOVA; main effect of pancreatectomy ***p<0.001, main effect of isoprenaline treatment ##p<0.01. GLUT: glucose transporter, MHC: myosin heavy chain. SERCA: sarco/endoplasmic reticulum Ca2+-ATPase, UCP: Uncoupling protein.

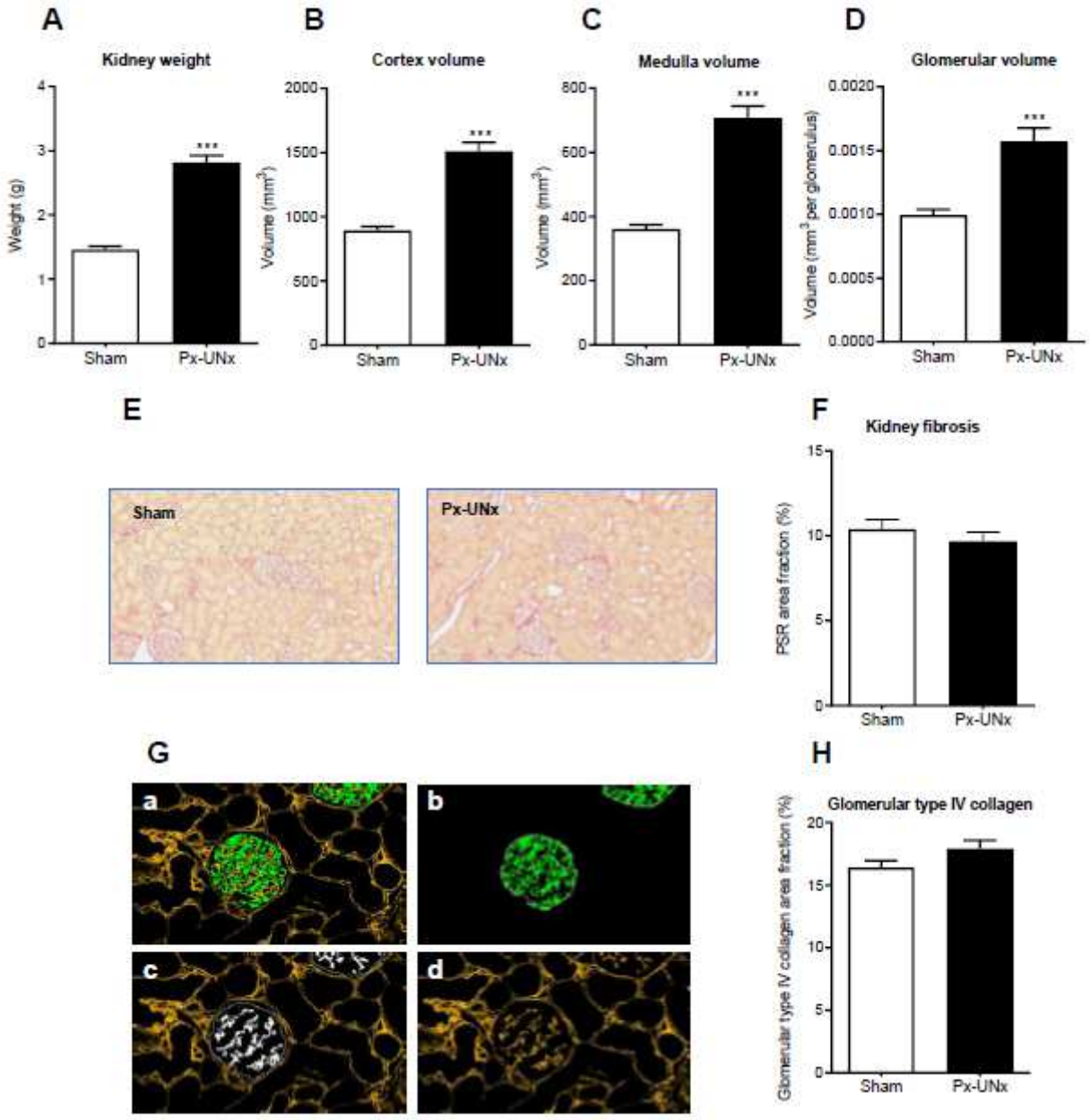

Figure 5

Renal morphometric and histopathological characteristics in pancreatectomized-uninephrectomized rats. Measurements were performed eleven weeks after sham or pancreatectomy-uninephrectomy (Px-UNx). Kidney weight and volume of renal compartments (A-D). Representative images of Picro Sirius Red (PSR) stained kidney sections and total renal fibrosis quantification (E-F). Representative images of kidney sections stained for co-localization type IV collagen (yellow) and podocin (green), and quantification of intra-glomerular type IV collagen (white) (G-H). Data is presented as mean + SEM. n=11-12 in each group. Unpaired t-test; ***p<0.001 vs. sham.

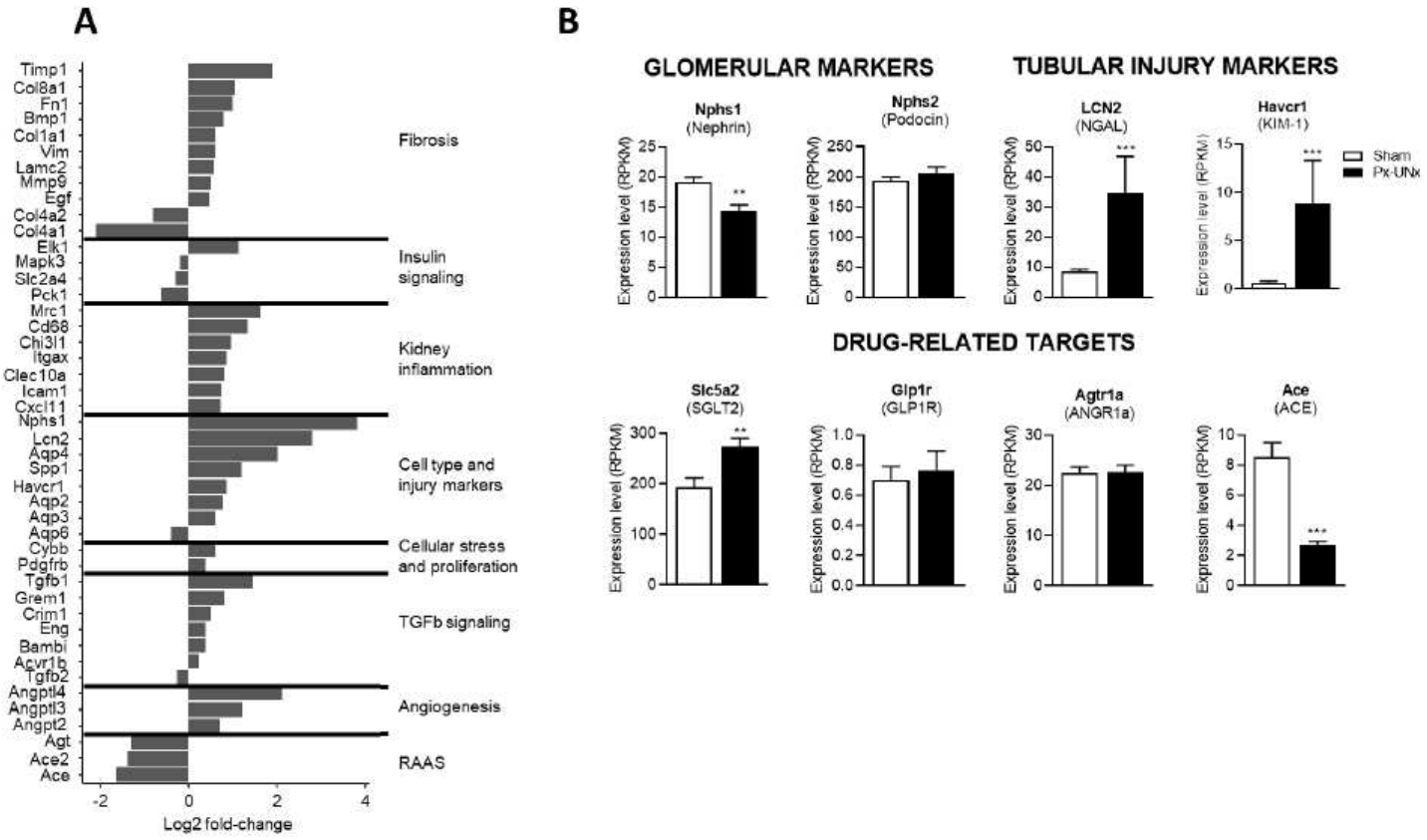

Figure 6

Renal gene expression in pancreatectomized-uninephrectomized rats. Measurements were performed at termination, eleven weeks after sham or pancreatectomy-uninephrectomy (Px-UNx). Pathway summary presenting selected genes that are significantly regulated in the renal cortex of Px-UNx vs. Sham animals at p<0.01 significance level (A). Expression levels of selected genes in the renal cortex (B). Data are mean + SEM (n=11-12). Unpaired t-test; **p<0.01, **p<0.001 vs Sham after correction for gene-wise multiple testing. ACE: Angiotensin I converting enzyme, ANGR1a: Angiotensin II receptor, type 1a, GLP1R: Glucagon-like peptide 1 receptor, KIM-1: kidney injury molecule 1, NGAL: neutrophil gelatinase-associated lipocalin, RAAS: renin-angiotensin-aldosterone system, SGLT2: Sodium-glucose transport protein 2.